JOURNAL
OF THE AMERICAN CHEMICAL SOCIETY

VOLUME 98, NUMBER 26 DECEMBER 22, 1976

Statistical Phase Space Theory of Polyatomic Systems. Application to the Cross Section and Product Kinetic Energy Distribution of the Reaction $C_2H_4^{\cdot+} + C_2H_4 \rightarrow C_3H_5^+ + CH_3\cdot$

W. J. Chesnavich and M. T. Bowers*

Contribution from the Department of Chemistry, University of California, Santa Barbara, California 93106. *Received March 22, 1976*

Abstract: The statistical phase space theory is developed for the bimolecular reaction of two polyatomic species. Formulas are obtained for the energy dependence of the cross section and for the product kinetic energy distribution resulting from a bimolecular collision event. Rigorous conservation of energy and angular momentum is adhered to. The theory is applied to the reaction $C_2H_4^{\cdot+} + C_2H_4 \rightarrow C_3H_5^+ + \cdot CH_3$ and compared with experimental results. The experimental cross section (Le Breton et al.) decreases much more rapidly with internal energy in the $C_2H_4^{\cdot+}$ ion than is predicted by theory. The result is explained by considering the characteristics of the potential surface in the region of the $C_4H_8^{\cdot+}$ intermediate complex. The experimental product kinetic energy distribution (Lee et al.) is well reproduced by theory over a range of $C_2H_4^{\cdot+}$ kinetic energies. This result contrasts with conclusions of Lee et al. that suggested vibrational energy was not randomized in the $C_4H_8^{\cdot+}$ collision complex. The diagnostic usefulness of phase space theory is emphasized.

I. Introduction

One of the fundamental objectives of chemical dynamics is the understanding of the state dependence of rate constants or cross sections of chemical reactions. Recent experiments that are beginning to give us information of this sort include reactive scattering in molecular beams,[1] chemiluminescence from products of chemical reactions,[2] unimolecular fragmentation of ions with fixed amounts of internal energy,[3] variation of reaction cross sections with reactant ion internal energy,[4] and velocity distribution of reaction products from unimolecular[5] and bimolecular reactions.[6] Ideally, theoretical approaches that are based on solutions to the Schrödinger equation, or at least on trajectory calculations given an energy surface, are desired. Such approaches are being applied to simple systems with some success.[7] It appears that such theories will not be generally useful for systems comprising more than three or four atoms, however, so other methods must be developed. Most other methods have their roots in activated complex theory[8] or the related RRKM theory.[9] These statistical approaches to chemical reactions have been very useful for interpreting unimolecular reactions in neutral systems.[10] However, the fact that they do not explicitly conserve angular momentum limits their utility in bimolecular collision systems. This restriction is particularly severe for low-energy ion–molecule reactions where very large impact parameter collisions dominate the cross section.

Light and co-workers[11] and Nikitin[12] first successfully included angular momentum conservation in statistical molecular collision theory. Both quantum and classical forms of the theory, usually called phase space theory, have been developed and primarily applied to three-atom systems. The theory has been extended to include two diatomic molecules[12-14] and an atom interacting with a prolate or oblate spheroid.[12,13]

Initial attempts to extend phase space theory to polyatomic systems limited themselves to approximate treatments. Klots[15] developed a formalism for a number of reactant pairs including two spherical species in the limit of zero total angular momentum, and hence its usefulness is limited to unimolecular reactions. In addition, he recently developed an approximate method suitable for use in the high total angular momentum limit.[15b] Safron et al.[16] developed an approximate "loose transition state" theory under the assumption that the total system angular momentum is transferred to orbital angular momentum of the products. Marcus[17] has extended "tight transition state" theory to the cases where the total system angular momentum passes either totally to orbital or totally to internal angular momentum of the products.

Recently we have developed techniques for rigorously calculating sums of states and densities of states of certain polyatomic systems under the restraints of conservation of energy and conservation of angular momentum.[18] The systems covered to date include pairwise interactions of a spherical top molecule with either a linear molecule or a spherical, prolate, or oblate top molecule as a partner. In this paper we develop the necessary formalism for applying these sums and densities of states to the calculation of reaction cross sections and product kinetic energy distributions. The results are then ap-

plied to the reaction

$$C_4H_4{\cdot}^+ + C_2H_4 \rightarrow C_3H_5^+ + CH_3{\cdot}$$

Comparison will be made with the experimental results of Le Breton et al.[4b] who have recently measured the energy dependence of the cross section using photoionization techniques. The experimental product translational energies have been reported by Lee et al.[6,19] as a function of $C_2H_4{\cdot}^+$ translational energy using a crossed molecular beam device and comparison will be made with these results. The discussion of the comparison of theory with experiment will center on the mechanism of the reaction, in particular the question of whether or not energy is randomized in the collision complex.

II. Theory

Consider a bimolecular reaction proceeding from reactants in channel a to products in channel b. The essence of the statistical theory is the assumption that reaction proceeds through resonance states in which there is strong coupling of all degrees of freedom. Strong coupling effectively allows a collision event to be separated into two distinct processes, complex formation and complex decay. These two processes are uncoupled except through energy and momentum conservation laws. Therefore the reaction cross section may be written as[11]

$$\sigma(a\rightarrow b) = \int \frac{\partial\sigma(a\rightarrow\mathcal{J})}{\partial\mathcal{J}} P(\mathcal{J}\rightarrow b)\, d\mathcal{J} \qquad (1)$$

It is important to note that in eq 1 "a" represents a particular state or average over states in the incoming channel and "b" a particular state or sum over states in the outgoing channel. The partial capture cross section from reactants to the complex with total angular momentum $\mathcal{J}$ is given by $\partial\sigma(a\rightarrow\mathcal{J})/\partial\mathcal{J}$ and $P(\mathcal{J}\rightarrow b)$ is the decomposition probability to channel b. The decomposition probability is taken as the ratio of phase space available to b divided by the total phase space available to the complex under the restraints imposed by conservation of energy and angular momentum.

The methods commonly used to estimate $\partial\sigma(a\rightarrow\mathcal{J})/\partial\mathcal{J}$ are well known[11,17] and will be briefly reviewed in subsection B. There, we will also discuss the effect of reaction path degeneracy[20] on eq 1. However, first we shall take on a more formidable task, the determination of the accessible phase space in bimolecular systems consisting of two polyatomic species. A geometric approach to this problem, presented elsewhere,[18] provides the best method when one or both of the molecules are oblate or prolate symmetric tops. We have found, however, that in most cases adequate approximations to system phase space are obtained when three-dimensional rotors are treated as spherical tops.[18] We therefore present in subsection A a brief but concise derivation of the equations used to determine system phase space for bimolecular systems consisting of a spherical top molecule paired with either a spherical top or a linear molecule. A glossary of important terms is given in Table I for the reader's convenience.

Table I. Glossary of Important Terms[a]

$\mathcal{J}$	System total angular momentum
L	Orbital angular momentum
J_r	Total rotational angular momentum
E	Energy above zero point of the potential energy surface
$\rho_v(\mathcal{E}_v)$	Vibrational density of states at vibrational energy, $\mathcal{E}_v$
$\mathcal{P}(\mathcal{E}_r,J_r)$	Rotational density of states at rotational energy $\mathcal{E}_r$ and total rotational angular momentum J_r
$\Gamma(\mathcal{E}_r{}^*,J_r)$	Rotational sum of states at rotational energy less than or equal to $\mathcal{E}_r{}^*$ and at total rotational angular momentum J_r
$\mathcal{P}(\mathcal{E}_t,\mathcal{E}_r,\mathcal{J})$	Rotational-orbital density of states at rotational energy $\mathcal{E}_r$, translational energy $\mathcal{E}_t$, and total angular momentum $\mathcal{J}$
$\Gamma(\mathcal{E}_{tr},\mathcal{J})$	Rotational-orbital sum of states at translational-rotational energy sum $\mathcal{E}_{tr}$ and at total angular momentum $\mathcal{J}$
$\Phi'(E,\mathcal{E}_t,\mathcal{J})$	Total phase space density of states at energy E of which energy $\mathcal{E}_t$ is translational and at total angular momentum $\mathcal{J}$
$\Phi(E,\mathcal{J})$	Total phase space sum of states at energy E and total angular momentum $\mathcal{J}$

[a] An asterisk on an energy or momentum symbol implies a maximum and a dagger superscript implies a minimum. The subscripts a and b are used when it is necessary to designate a particular reaction channel.

(A) The Determination of Accessible Phase Space in Bimolecular Systems Involving Spherical and Linear Polyatomic Species. In order to determine the total phase space available to a given reaction channel, we first make the assumption that E, the energy above the zero point of the potential energy surface in that channel, can be divided into the total vibrational energy $\mathcal{E}_v$ and the total translational-rotational energy sum, $\mathcal{E}_{tr}$

$$E = \mathcal{E}_v + \mathcal{E}_{tr}$$

This assumption allows the phase space to be separated into the contributions from system vibrational motion and system translational-rotational motion. The vibrational phase space is given semiclassically by the density of vibrational states $\rho_v(\mathcal{E}_v)\, d\mathcal{E}_v$. If we let $\Gamma(\mathcal{E}_{tr},\mathcal{J})$ be the system translational-rotational phase space, or momentum space, the total system phase space is, then

$$\Phi(E,\mathcal{J}) = \int_{\mathcal{E}_{tr}{}^\ddagger}^{E} \rho_v(E-\mathcal{E}_{tr})\Gamma(\mathcal{E}_{tr},\mathcal{J})\, d\mathcal{E}_{tr} \qquad (2)$$

The lower limit $\mathcal{E}_{tr}{}^\ddagger$ is a function of $\mathcal{J}$ and will be determined later.

If we are interested in the total system phase space at a constant translational energy, $\mathcal{E}_{tr}$ must be separated into the system translational energy, $\mathcal{E}_t$, and system rotational energy, $\mathcal{E}_r$

$$\mathcal{E}_{tr} = \mathcal{E}_t + \mathcal{E}_r \qquad (3)$$

If $\mathcal{P}(\mathcal{E}_t,\mathcal{E}_r,\mathcal{J})\, d\mathcal{E}_t$ is the total system momentum space at constant $\mathcal{E}_t$ and $\mathcal{E}_r$, the total system phase space at constant $\mathcal{E}_t$ is

$$\Phi'(E,\mathcal{E}_t,\mathcal{J})\, d\mathcal{E}_t = d\mathcal{E}_t \int_{\mathcal{E}_r{}^\ddagger}^{E-\mathcal{E}_t} \rho(E-\mathcal{E}_t-\mathcal{E}_r)\mathcal{P}(\mathcal{E}_t,\mathcal{E}_r,\mathcal{J})\, d\mathcal{E}_r \qquad (4)$$

The lower limit $\mathcal{E}_r{}^\ddagger$ is a function of both $\mathcal{E}_t$ and $\mathcal{J}$. This limit will also be determined later.

In order to determine $\Gamma(\mathcal{E}_{tr},\mathcal{J})$ and $\mathcal{P}(\mathcal{E}_t,\mathcal{E}_r,\mathcal{J})$ we must treat the vector addition of three angular momenta. The method used is not new.[14] We first couple the rotational angular momenta $\mathbf{J}_1$ and $\mathbf{J}_2$ to form a resultant $\mathbf{J}_r$:

$$\mathbf{J}_1 + \mathbf{J}_2 = \mathbf{J}_r \qquad (5a)$$

The vector $\mathbf{J}_r$ is then coupled with $\mathbf{L}$ to form the total angular momentum, $\mathcal{J}$:

$$\mathbf{J}_r + \mathbf{L} = \mathcal{J} \qquad (5b)$$

This separation of momenta is actually a separation of the system orbital motion and rotational motion. The vector $\mathbf{J}_r$ simply describes the spatial orientation of $\mathbf{J}_1$ relative to $\mathbf{J}_2$.

Consider now a bimolecular system of either two spheres or a sphere and linear molecule with total rotational energy, $\mathcal{E}_r$. The rotational angular momenta $\mathbf{J}_1$ and $\mathbf{J}_2$ are related to $\mathcal{E}_r$ by

$$\mathcal{E}_r = B_1 J_1^2 + B_2 J_2^2 \tag{6a}$$

where B_1 and B_2 are the molecular rotational constants. For a total rotational angular momentum J_r, J_1 and J_2 must lie in the range

$$|J_1 - J_2| \leq J_r \leq J_1 + J_2 \tag{6b}$$

and for each spherical top the range of K, the projection of J on the internal symmetry axis, is

$$-J \leq K \leq J \tag{6c}$$

The rotational phase space volume element for two spheres is

$$d\Gamma = dK_1\, dK_2\, dJ_1\, dJ_2 \tag{7a}$$

For a sphere and linear molecule the volume element becomes

$$d\Gamma = dK_s\, dJ_s\, dJ_l \tag{7b}$$

In order to determine the system rotational phase space, eq 7a and 7b must be integrated with respect to each angular momentum variable over the range allowed by the restrictions imposed by (6a)-(6c). This integration will be demonstrated for the sphere-sphere system.

In order to integrate (7a) under the restraint imposed by (6a) the integral must be transformed to the hypersurface of constant rotational energy. This result is accomplished by using the Jacobian to convert one variable in the volume element (7a) to the differential $d\mathcal{E}_r$. Choosing J_2 to be converted, the Jacobian is, from (6a),

$$\partial J_2/\partial \mathcal{E}_r = (2B_2J_2)^{-1}$$

and (7a) becomes

$$d\Gamma = dK_1\, dK_2(\partial J_2/\partial \mathcal{E}_r)\, d\mathcal{E}_r\, dJ_1 = \frac{d\mathcal{E}_r}{2B_2}\frac{dK_1\, dK_2\, dJ_1}{J_2} \tag{8}$$

The integrations of eq 8 can now be performed. The result, $\mathcal{P}(\mathcal{E}_r,J_r)$, is the density of rotational states of a bimolecular system of two spheres with total rotational energy $\mathcal{E}_r$ and total rotational angular momentum J_r. Since K_1 and K_2 are not energy dependent, eq 8 can be integrated over K_1 and K_2 using (6c):

$$\mathcal{P}(\mathcal{E}_r,J_r)\, d\mathcal{E}_r = \frac{d\mathcal{E}_r}{2B_2}\int\int \frac{2J_1\, dK_2\, dJ_1}{J_2} = \frac{d\mathcal{E}_r}{B_2}\int 2J_1\, dJ_1 \tag{9}$$

The boundaries on J_1 must be determined. Consider Figure 1. The constant energy surface defined by (6a) is given as curve A. For a particular J_r we are restricted by momentum conservation to that part of the curve within the rectangular boundaries given by (6b). The limits of (6b) can be substituted into (6a) to determine $J_\pm$, the values of J_1 at the intersections:

$$J_\pm = \frac{|(\omega\mathcal{E}_r - B_1B_2J_r^2)^{1/2} - B_2J_\pm|}{\omega} \tag{10}$$

In eq 10, $\omega = B_1 + B_2$. Using these limits, eq 9 can be integrated over J_1 to obtain $\mathcal{P}(\mathcal{E}_r,J_r)$:

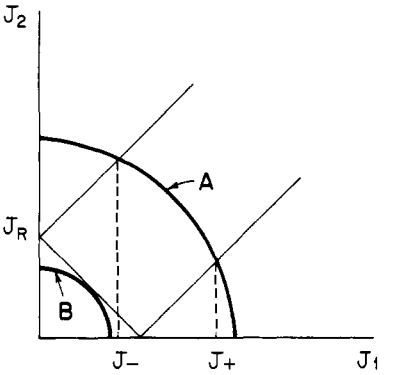

Figure 1. Boundaries in the J_1-J_2 plane. The rectangular boundaries are imposed by eq 5a and curves A and B refer to eq 6a. Curve B represents the minimum rotational energy for which there is available system phase space.

$$\mathcal{P}(\mathcal{E}_r,J_r)\, d\mathcal{E}_r = \frac{d\mathcal{E}_r}{B_2}\int_{J_-}^{J_+} 2J_1\, dJ_1 = \frac{d\mathcal{E}_r}{B_2}[J_+^2 - J_-^2] = \frac{4J_r}{\omega^2}[\omega\mathcal{E}_r - B_1B_2J_r^2]^{1/2}\, d\mathcal{E}_r \tag{11}$$

The sum of states for energy less than or equal to the maximum allowed energy, $\mathcal{E}_r^*$, can also be determined. The minimum value of $\mathcal{E}_r$ for a given J_r is determined by setting $\mathcal{P}(\mathcal{E}_r,J_r) = 0$ in (11)

$$\mathcal{E}_m = B_rJ_r^2 \tag{12}$$

where B_r is the system reduced moment of inertia, B_1B_2/ω. This minimum energy describes curve B in Figure 1. Integration of eq 11 over all allowed rotational energies yields the sum of states:

$$\Gamma(\mathcal{E}_r^*,J_r) = \int_{B_rJ_r^2}^{\mathcal{E}_r^*} \mathcal{P}(\mathcal{E}_r,J_r)\, d\mathcal{E}_r = \frac{8J_r}{3\omega^3}(\omega\mathcal{E}_r^* - B_1B_2J_r^2)^{3/2} \tag{13}$$

Using exactly the same procedure eq 7b can be integrated for the sphere-linear system. The results are

$$\mathcal{P}(\mathcal{E}_r,J_r) = 2J_r/\omega \qquad \mathcal{E}_r \geq B_sJ_r^2 \tag{14a}$$

$$= \frac{2}{B_s\omega}[\omega\mathcal{E}_r - B_sB_lJ_r^2]^{1/2} \qquad \mathcal{E}_r \leq B_sJ_r^2 \tag{14b}$$

$$\Gamma(\mathcal{E}_r^*,J_r) = \frac{2J_r}{\omega^2}[\omega\mathcal{E}_r^* - B_s(B_l + B_s/3)J_r^2] \qquad \mathcal{E}_r^* \geq B_sJ_r^2 \tag{15a}$$

$$= \frac{4}{3B_s\omega^2}[\omega\mathcal{E}_r^* - B_sB_lJ_r^2]^{3/2} \qquad \mathcal{E}_r^* \leq B_sJ_r^2 \tag{15b}$$

In order to determine $\Gamma(\mathcal{E}_{tr},\mathcal{J})$ and $\mathcal{P}(\mathcal{E}_t,\mathcal{E}_r,\mathcal{J})$, the sum of states $\Gamma(\mathcal{E}_r^*,J_r)$ and density of states $\mathcal{P}(\mathcal{E}_r,J_r)$ must be integrated in the L-J_r plane. In this paper we will consider only the sphere-sphere system for ion-molecule reactions. For an ion-molecule interaction potential of the form $V_r = -\alpha q^2/2r^4$, and for a given translational energy $\mathcal{E}_t$, the maximum orbital angular momentum capable of overcoming the centrifugal barrier is[21]

$$L^* = (\Lambda\mathcal{E}_t)^{1/4} \tag{16}$$

where

$$\Lambda = 8\mu^2q^2\alpha/\hbar^4$$

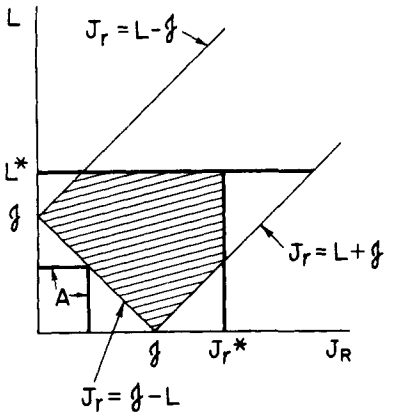

Figure 2. Range of integration in the L–J_r plane for $\mathcal{P}(\mathcal{E}_t,\mathcal{E}_r,\mathcal{J})$.

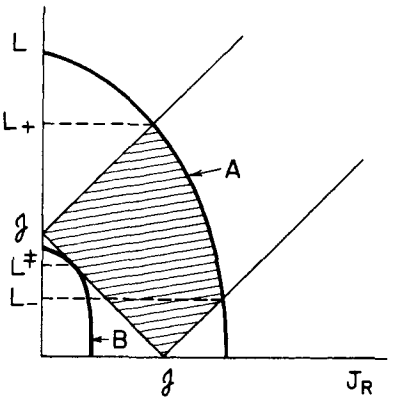

Figure 3. Range of integration in the L–J_r plane for $\Gamma(\mathcal{E}_t,\mathcal{J})$. Curve A is the boundary given by eq 14. The symbols are explained in the text.

Here, μ is the reduced mass, q is the ion charge, and α is the polarizability of the neutral. In order to determine $\mathcal{P}(\mathcal{E}_t,\mathcal{E}_r,\mathcal{J})$, the density of states $\mathcal{P}(\mathcal{E}_r,J_r)$ must be integrated in the L–J_r plane within the boundaries given by (5b), (12), and (16). An example of the region of integration is given in Figure 2. For a given $\mathcal{E}_r$, J_r^* is obtained from eq 12 as

$$J_r^* = (\mathcal{E}_r/B_r)^{1/2} \tag{17}$$

For the region shown in Figure 2, $\mathcal{P}(\mathcal{E}_t,\mathcal{E}_r,\mathcal{J})$ is

$$\begin{aligned}\mathcal{P}(\mathcal{E}_t,\mathcal{E}_r,\mathcal{J}) &= \int_0^{J_r^*-\mathcal{J}} \int_{|\mathcal{J}-L|}^{\mathcal{J}+L} \mathcal{P}(\mathcal{E}_r,J_r)\,dJ_r\,dL \\ &\quad + \int_{J_r^*-\mathcal{J}}^{L^*} \int_{|\mathcal{J}-L|}^{J_r^*} \mathcal{P}(\mathcal{E}_r,J_r)\,dJ_r\,dL \\ &= 2H(\mathcal{J}) + H(L^*-\mathcal{J}) - \pi\mathcal{E}_r^2/4(B_1B_2)^{3/2} \end{aligned} \tag{18}$$

where

$$\begin{aligned}H(X) = X\frac{(\omega\mathcal{E}_r - B_1B_2X^2)^{1/2}}{3B_1B_2\omega^2}(5\omega\mathcal{E}_r/2 - B_1B_2X^2) \\ + \mathcal{E}_r^2/(B_1B_2)^{3/2}\sin^{-1}X/J_r^*\end{aligned}$$

There are five distinct results for $\mathcal{P}(\mathcal{E}_t,\mathcal{E}_r,\mathcal{J})$ depending on the relative values of L^*, J_r^*, and $\mathcal{J}$ for the sphere–sphere system and, due to the boundary at $\mathcal{E}_r = B_sJ_r^2$, there are 17 results for the sphere–linear system. The entire set is presented elsewhere.[18]

In order to determine $\Gamma(\mathcal{E}_{tr},\mathcal{J})$ we must consider a translational-rotational energy term $\mathcal{E}_{tr}$. For a given L eq 16 can be inverted to give $\mathcal{E}_t^{\ddagger}$, the minimum translational energy capable of overcoming the centrifugal barrier;

$$\mathcal{E}_t^{\ddagger} = L^4/\Lambda \tag{19}$$

Equations 3 and 17 can be combined to determine $\mathcal{E}_r^*$, the rotational energy maximum for a given L;

$$\mathcal{E}_r^* = \mathcal{E}_{tr} - L^4/\Lambda \tag{20}$$

Equations 3, 12, and 17 also determine an energy boundary in the L–J_r plane;

$$L^4/\Lambda + B_rJ_r^2 \le \mathcal{E}_{tr} \tag{21}$$

This boundary is portrayed by curve A in Figure 3. The integration of $\Gamma(\Gamma_r^*,J_r)$ within the boundaries given by (5b) and (21) gives the total rotational-orbital phase space, $\Gamma(\mathcal{E}_{tr},\mathcal{J})$.

For example, consider the integration of $\Gamma(\mathcal{E}_r^*,J_r)$ for the sphere–sphere system over the region shown in Figure 3. This integration is performed in the following manner

$$\begin{aligned}\Gamma(\mathcal{E}_{tr},\mathcal{J}) &= \int_0^{L_-} \int_{|\mathcal{J}-L|}^{\mathcal{J}+L} \Gamma(\mathcal{E}_r^*,J_r)\,dJ_r\,dL \\ &\quad + \int_{L_-}^{L_+} \int_{|\mathcal{J}-L|}^{(\mathcal{E}_r^*/B_r)^{1/2}} \Gamma(\mathcal{E}_r^*,J_r)\,dJ_r\,dL \\ &= \frac{8}{15B_1B_2\omega^3}\int_0^{L_+}[\omega\mathcal{E}_r^* - B_1B_2(\mathcal{J}-L)^2]^{5/2}\,dL \\ &\quad - \int_0^{L_-}[\omega\mathcal{E}_r^* - B_1B_2(\mathcal{J}+L)^2]^{5/2}\,dL \end{aligned} \tag{22}$$

In (22) $\mathcal{E}_r^*$ is given by (20) and $L_{\pm}$ are the intersections of (19) with the momentum boundaries given by (5b). Numerical techniques must be used both to solve for $L_{\pm}$ and to evaluate the integrals in (22).

Using results such as (18) and (22), the total system phase space, eq 2 and 4 can now be evaluated. The minimum $\mathcal{E}_{tr}^{\ddagger}$, illustrated by curve B in Figure 3, is determined in the following manner. First, eq 21 is differentiated with respect to J_r, yielding (23a);

$$(4L^3/\Lambda)\,\partial L/\partial J_r + 2B_rJ_r = 0 \tag{23a}$$

When $\mathcal{E}_{tr} = \mathcal{E}_{tr}^{\ddagger}$, $\partial L/\partial J = -1$, $L = L^{\ddagger}$, and J_r is determined from the momentum boundary as $J_r = \mathcal{J} - L^{\ddagger}$. Making these substitutions into (23a) yields,

$$2L^{\ddagger 3}/B_r\Lambda + L^{\ddagger} - \mathcal{J} = 0$$

which can be solved to give

$$L^{\ddagger} = \left(\frac{B_r\Lambda}{2}\right)^{1/3}\{(S + \mathcal{J}/2)^{1/3} - (S - \mathcal{J}/2)^{1/3}\} \tag{23b}$$

where

$$S = (\mathcal{J}^2/4 + B_r\Lambda/54)^{1/2}$$

Finally, $L^{\ddagger}$ from (23b) can be substituted back into (21) to give

$$\mathcal{E}_{tr}^{\ddagger} = L^{\ddagger 4}/\Lambda + B_r(\mathcal{J} - L^{\ddagger})^2 \tag{23c}$$

For neutral–neutral reactions with an interaction potential of the form $-C/r^6$ similar considerations apply.

The minimum $\mathcal{E}_r^{\ddagger}$ is given as curve A in Figure 2 for $\mathcal{J} \le L^*$. In this case $\mathcal{E}_r^{\ddagger}$ is

$$\mathcal{E}_r^{\ddagger} = B_r(\mathcal{J} - L^*)^2 \tag{24}$$

If $\mathcal{J} \ge L^*$ the minimum rotational energy in (4) is zero.

(B) Determination of the Statistical Reaction Cross Section. Now that we have determined $\Gamma(\mathcal{E}_{tr},\mathcal{J})$ and $\mathcal{P}(\mathcal{E}_t,\mathcal{E}_r,\mathcal{J})$ we can use them in (2) and (4) to calculate the total system phase space for each reaction channel. The total phase space for each

channel determines the decomposition probability $P(\mathscr{J}\rightarrow b)$. The decomposition probability, coupled with the partial capture cross section, in turn allows us to evaluate (1).

Let us first consider the partial capture cross section $\partial\sigma(a\rightarrow\mathscr{J})/\partial\mathscr{J}$. In order to calculate this quantity the coupling of three reactant angular momenta L_a, J_{1a}, and J_{2a} must be treated. As is customary,[11,17] we assume that for most collisions L_a is much larger than the rotational momenta. This assumption will in general be valid for reactions dominated by large intermolecular potentials such as ion–neutral reactions or in beam reactions in which supersonic nozzle expansion is used to enhance translational energy at the expense of internal energy. The result of this assumption is that the system total angular momentum, $\mathscr{J}$, is considered to be generated entirely by L_a. We may therefore combine the classical collision theory relationships $d\sigma = 2\pi b\, db$ and $\mathscr{J}\hbar = \mu b v$ to obtain

$$\frac{\partial\sigma(a\rightarrow\mathscr{J})}{d\mathscr{J}} = \frac{\pi\hbar^2}{\mu\mathscr{E}_t^a}\mathscr{J} \tag{25}$$

In these equations b is the impact parameter, v is the incoming velocity and $\mathscr{E}_t^a$ the corresponding translational energy, μ is the reduced mass of the reactants, and $\mathscr{J}$ is expressed in units of $\hbar$. We can now substitute (25) into (1) to obtain

$$\sigma(a\rightarrow b) = \frac{\pi\hbar^2}{\mu\mathscr{E}_t^a}\int_0^{L_a^*}\mathscr{J}P(\mathscr{J}\rightarrow b)\,d\mathscr{J} \tag{26}$$

It remains to analytically define $P(\mathscr{J}\rightarrow b)$, the decomposition probability of the complex to state b. This probability must be defined so that the sum of probabilities to all channels equals unity and in such a way that the reaction path degeneracy of each channel is properly accounted for. (We use channel to signify a chemically distinct set of molecules.) The reaction path degeneracy of a channel is directly related to S, the product of the symmetry numbers of the individual molecular species in that channel.[20]

We define $P(\mathscr{J}\rightarrow b)$ in the following manner. According to eq 1 the entire collision process may be viewed in terms of two disjointed events: the formation of a collision complex and its subsequent unimolecular decay. Consider therefore a collision complex X which may decay into any one of a number of channels. For the bth channel

$$X \xrightarrow{k_b} b$$

where k_b is the unimolecular rate constant. The decomposition probability to channel b is

$$P(\mathscr{J}\rightarrow b) = k_b/\sum_i k_i \tag{27}$$

The application of phase space theory to the calculation of unimolecular decay rates shows that k_b is of the form[15,22]

$$k_b = S_X\Phi(E_b,\mathscr{J})/S_b h\rho_X(E_X) \tag{28}$$

where $\Phi(E_b,\mathscr{J})$ is given by eq 2 and the quantity $\rho_X(E_X)$ is the density of states of X. We substitute (28) into (27) to obtain

$$P(\mathscr{J}\rightarrow b) = \frac{\Phi(E_b,\mathscr{J})/S_b}{N_{TOT}} \tag{29}$$

where

$$N_{TOT} = \sum_i \Phi(E_i,\mathscr{J})/S_i$$

which correctly takes into account the effect of reaction path degeneracy.

Note also that summing eq 26 over all reaction paths gives

$$\sigma_{TOT} = \frac{\Pi\hbar^2}{\mu\mathscr{E}_t^a}\int_0^{L_a^*}\mathscr{J}\sum_i P_i(\mathscr{J}\rightarrow i)\,d\mathscr{J} = \pi\hbar^2 L_a^{*2}/2\mu\mathscr{E}_t^a \tag{30}$$

which is just the Langevin capture cross section. Hence, reaction path degeneracy contributes to the available phase space of a specific channel but, as expected, it does not enter into the total capture cross section.

To obtain the differential cross section for a specific product translational energy, eq 26 remains the same but the decomposition probability (29) becomes

$$P(\mathscr{J}\rightarrow\mathscr{E}_t^b) = \frac{d\mathscr{E}_t^b\Phi'(E_b,\mathscr{E}_t^b,\mathscr{J})/S_b}{\sum_i\Phi(E_i,\mathscr{J})/S_i} \tag{31}$$

where $\Phi'(E,\mathscr{E}_t^b,\mathscr{J})$ is given by eq 4. The product translational energy distribution is simply

$$P(\mathscr{E}_t^b)\,d\mathscr{E}_t^b = \sigma(a\rightarrow\mathscr{E}_t^b)\,d\mathscr{E}_t^b/\sigma_{TOT} \tag{32}$$

where σ_{TOT} is given by eq 30.

III. Results and Discussion

The theory outlined in the previous section will be applied to the reaction

$$C_2H_4{\cdot}^+ + C_2H_4 \rightarrow C_3H_5^+ + CH_3{\cdot}$$

and comparison made with experimental data. The dependence of the cross section on internal energy of $C_2H_4{\cdot}^+$ will be discussed first and the distribution of kinetic energies of the products as a function of $C_2H_4{\cdot}^+$ translational energy will be discussed second.

(A) Dependence of the Cross Section on Internal Energy in $C_2H_4{\cdot}^+$. Both the experimental data and the theoretical calculations are summarized in Figures 4 and 5. The photoionization data of Le Breton et al.[4b] were obtained in a single-source high-pressure photoionization mass spectrometer. Interested readers are referred to that paper for a thorough discussion of the experimental technique and the method of data reduction used to obtain the points plotted in our Figure 4 (see Figure 7 of ref 4b). Of importance are the facts that these data were recorded at 10% conversion and the repeller field was 4 V yielding an average ion translational energy at the exit slit of ca. 3 eV. At the pressure of the experiment the time between collisions is ca. 5×10^{-6} s.

The data in Figure 5 represent the direct dependence of the reaction cross section on internal energy in the $C_2H_4{\cdot}^+$ ion, as supplied by Williamson.[23] They were obtained from photoionization data similar to that presented in Figure 4.

The phase space calculations in Figures 4 and 5 were obtained from eq 26 and 29 and the data in Table II.[24] In Figure 5, the energies used to obtain the calculated curve are simply given as the abscissa. In Figure 4, the probability a reactant $C_2H_4{\cdot}^+$ ion contained a particular internal energy at a given photon energy was assumed to be given by the energy deposition function. For the purposes of this paper, this function was assumed to be adequately represented by the photoelectron spectrum.[25,26] The velocity distribution of the ions in the photoionization instrument was calculated using known techniques.[21] The theoretical results in Figures 4 and 5 were relatively insensitive to this distribution, presumably because relative quantities are considered in both cases.

The comparison between theory and experiment is interesting. In Figure 4, the qualitative shape of the theoretical line is very similar to the shape of a curve that could be drawn through the photoionization data points. In particular, a break in the curve is apparent at the onset of the $^2B_3$ electronic state of $C_2H_4{\cdot}^+$. The break in the theoretical curve at this point is

Table II. Parameters Used in Phase Space Calculations in the Reaction $C_2H_4^{\cdot+} + C_2H_4 \rightarrow C_3H_5^+ + CH_3\cdot$

Species	Rotational constants, cm^{-1} A	B	C	⟨G.M.⟩,[a] cm^{-1}	$\alpha \times 10^{24}$ cm^3	$\Delta H_f°_{298}$, kcal/mol
C_2H_4	4.828	1.001	0.828	1.588	4.22[b]	12.5[c]
$C_2H_4^{\cdot+}$	4.828	1.001	0.828	1.588		253[d]
CH_3	1.531	0.298	0.249	0.484	2.20[b]	34.8[c]
$C_3H_5^+$	9.631	9.631	4.816	7.644		226[e]

Vibrational frequency distributions, cm^{-1}			
$C_2H_4^{\cdot+} + C_2H_4$[f]	$C_2H_4^{\cdot+} + CH_2H_4$[f]	$C_3H_5^+ + CH_3\cdot$[g]	$C_3H_5^+ + CH_3\cdot$[g]
3300 (2)	1000 (4)	3200 (2)	1200 (4)
3100 (2)	900 (4)	3100 (2)	1000 (1)
3000 (4)	800 (2)	3000 (4)	900 (1)
1600 (2)		2000 (1)	800 (1)
1400 (2)		1400 (4)	600 (1)
1300 (2)		1300 (1)	400 (2)

[a] Geometric mean of the three rotational constants. [b] A. T. Amos and R. J. Crespin, *J. Chem. Phys.*, **63**, 1890 (1975). [c] D. R. Stull and H. Prophet, *Natl. Stand. Ref. Data Ser., Natl. Bur. Stand.*, **No. 37** (1971). [d] J. L. Franklin, J. G. Dillard, H. M. Rosenstock, J. T. Heron, K. Draxl, and F. H. Field, *Natl. Stand. Ref. Data Ser., Natl. Bur. Stand.*, **No. 26** (1969). [e] F. P. Lossing, *Can. J. Chem.*, **49**, 357 (1971); see also, S. E. Buttrill, Jr., A. D. Williamson, and P. Le Breton, *J. Chem. Phys.*, **62**, 1586 (1975). [f] The symmetry degeneracy of the $C_2H_4^{\cdot+} + C_2H_4$ reactants is $S = 4$. [g] The symmetry degeneracy of the $C_3H_5^+ + CH_3\cdot$ products is $S = 3$. The frequencies of CH_3 are 3100 (2), 3000 (1), 1400 (2), and 800 (1).

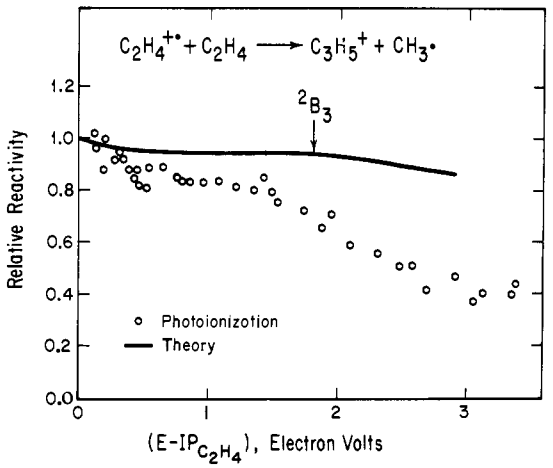

Figure 4. Relative reactivity of reaction 1 as a function of photoionization energy of the $C_2H_4^{\cdot+}$ ion. The solid line is the phase space calculation and the open circles the experimental photoionization results (ref 4b).

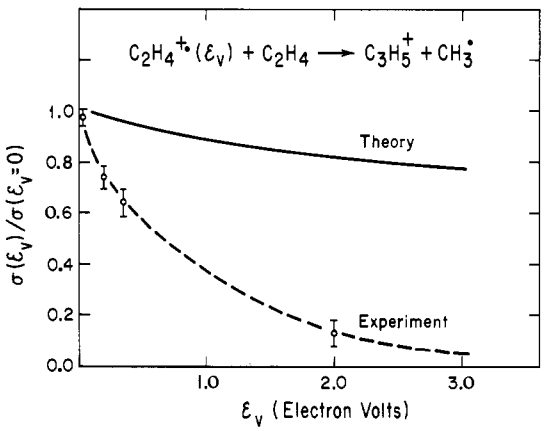

Figure 5. Relative reactivity of reaction 1 as a function of the internal energy in the $C_2H_4^{\cdot+}$ ion. The solid line is the phase space calculation. The circles are the experimental data (ref 23). The dashed line is a smooth curve drawn through the data points.

due to the increase in the energy deposition function as the $^2B_3$ state becomes energy accessible. The break in the experimental data must also, at least in part, reflect this fact. The lack of quantitative agreement between the experimental data and the phase space calculations is very clearly shown in Figure 5. The experimental cross section falls very much faster than theory as the $C_2H_4^{\cdot+}$ ion becomes internally excited. Note that no break occurs at the onset of the $^2B_3$ state in the theoretical curve in this figure because energy is a smoothly increasing function in the ion. It is also interesting and important that no apparent break occurs in experimental data at the onset of the $^2B_3$ state, although there are too few data points to be certain in this case. It does appear, however, that experimentally $\sigma(\mathcal{E}_v)/\sigma(\mathcal{E}_{v=0})$ is a smoothly decreasing function, in fact decreasing almost exactly exponentially.

The results are consistent with the following interpretation: The phase space calculations assume the energy dependence of the cross section depends only on the properties of the products and reactants. Clearly this assumption is not adequate to explain the data in the present case. The cross sectional energy dependence implies that the details of the potential surface in the region of the intermediate $C_4H_8\cdot^+$ ion are important. Following Le Breton et al.,[4b] we assume a tetramethylene ion is first formed in the collision of ethylene ion on ethylene neutral. The following reaction scheme is envisaged.

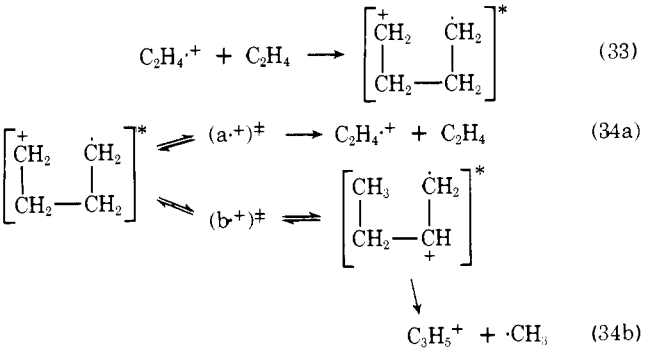

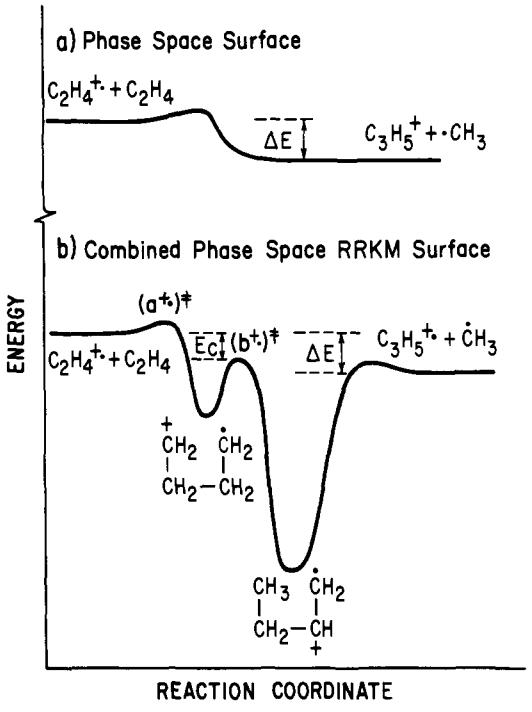

Figure 6. Schematic potential surface for reaction 1: (a) surface assumed for phase space calculations; (b) surface appropriate for combined phase space-RRKM calculation as discussed in the text. The reaction energy is ΔE and E_c is an energy associated with the isomerization barrier height. The symbols $(a\cdot^+)^{\ddagger}$ and $(b\cdot^+)^{\ddagger}$ represent the transition states for the two reaction pathways of the tetramethylene ion.

A schematic potential surface is given in Figure 6.

The tetramethylene ion, once formed, has two choices: either it can isomerize to form the more stable 1-butene ion or it can dissociate to reactants. The relative probability of these two processes will be determined by the energy and entropy associated with each path. The transition state for dissociation to reactants, $(a\cdot^+)^{\ddagger}$, will be characterized by high entropy as the process is envisioned as a simple C–C bond cleavage. The isomerization transition state, $(b\cdot^+)^{\ddagger}$, on the other hand, will be low entropy as it is envisioned as a cyclic structure. If the isomerization reaction occurs in one step, it would entail a 1-3 hydrogen shift and a four-member C–C–C–H ring.

The qualitative shapes of the k vs. E plots for the two reactions are shown in Figure 7.[27] The isomerization reaction has the lower threshold but rises more slowly with energy than the simple bond cleavage reaction. The experimentally accessible energy range begins near the threshold of the fragmentation reaction because this is the reverse of the reaction used to form the excited complex. As energy is increased the fragmentation reaction quickly becomes comparable in rate to the isomerization reaction and soon dominates the reactivity of the excited tetramethylene ion. The two dotted lines might represent the experimental energy range reported in Figure 5. If the reasonable assumption is made that the dissociation of the 1-butene ion to products is much faster than the back isomerization to tetramethylene ion,[28] then

$$\sigma(\mathcal{E}_v)/\sigma(\mathcal{E}_{v=0}) \cong \frac{k_b(\mathcal{E}_v)}{k_a(\mathcal{E}_v) + k_b(\mathcal{E}_v)}$$

The kind of curves drawn for $k_a(\mathcal{E}_v)$ and $k_b(\mathcal{E}_v)$ drawn in Figure 7, which are reasonable for the processes described, will clearly reproduce the experimental data of Figure 5.

This mechanism can be tested quantitatively but the theory for doing so is not yet complete. What must be done is to generate the tetramethylene intermediate ion via a collision between $C_2H_4\cdot^+$ and C_2H_4 conserving both energy and angular momentum. Then the relative rate constants for the two unimolecular reactions, $k_a(\mathcal{E}_v)$ and $k_b(\mathcal{E}_v)$, must be calculated from the set of tetramethylene ions with the energy and angular momentum distribution obtained via the formation collision. The first phase of this theory is complete.[29] The second, however, is still being developed. While it is speculative at this point to say such a treatment will quantitatively fit the data, our experience with a similar unimolecular reaction suggests it will.[30] A crucial parameter in the analysis will be the energy, E_c, that characterizes the isomerization barrier height. Since this quantity is unknown, it must be varied to best fit the data.

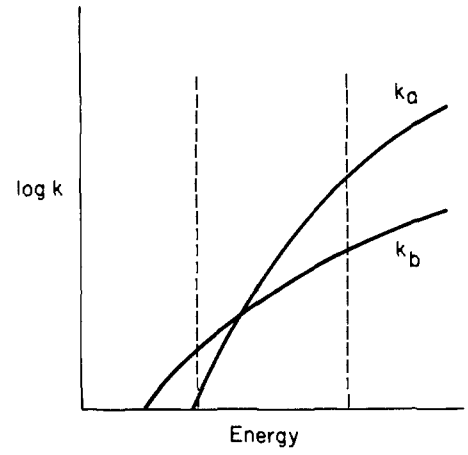

Figure 7. Hypothetical plot of log k vs. energy for the two reaction pathways (34a) and (34b). The vertical dashed lines give an energy range comparable to that given in Figure 5.

(B) The Product Kinetic Energy Distribution and Its Dependence on the Translational Energy of $C_2H_4\cdot^+$. The integrated product translational energy distributions at several $C_2H_4\cdot^+$ translational energies reported by Lee et al.[6] are given in Figure 8 as the open circles. These data were obtained in a crossed ion-neutral beam machine by integration of the velocity contours[19] over the complete velocity space. The $C_2H_4\cdot^+$ ions were formed in an electron impact source at 70 eV ionizing electron energy.

The phase space calculations are given as the solid lines in Figure 8. The solid curves are calculated by assuming half of the $C_2H_4\cdot^+$ ions have an internal energy of 0.25 eV while the other half have an internal energy of 2.11 eV. These values correspond to the average of the two major bands, having approximately equal intensity, in the photoion-photoelectron coincidence spectra[31] of C_2H_4 below the dissociation threshold of $C_2H_4\cdot^+$. One, of course, cannot accurately predict the internal energy of $C_2H_4\cdot^+$ ions formed under the conditions of the experiment but the method used here should not be greatly in error. The bars in the figure indicate the results of calculations done with all $C_2H_4\cdot^+$ ions with 2.11 eV internal energy (upper limit on bar) and with 0.25 eV (lower limit on bar). Other appropriate quantities used in the calculation are given in Table II.

The comparison with experiment is interesting. At lowest reactant ion energies the calculations agree with experiment for product ion energies up to ca. 0.6 eV and then slightly underestimate the probability for the high energy tail portion of the products. Similar agreement is found between calculation and experiment for the 2.21 eV reactant ion except some minor deviations begin to occur at ca. 0.4 eV product ion energy. Only when the reactant ion energies reach 3.26 eV does serious disagreement between experiment and theory begin to appear.

The lack of exact agreement between theory and experiment at the high product energies could occur for several reasons.

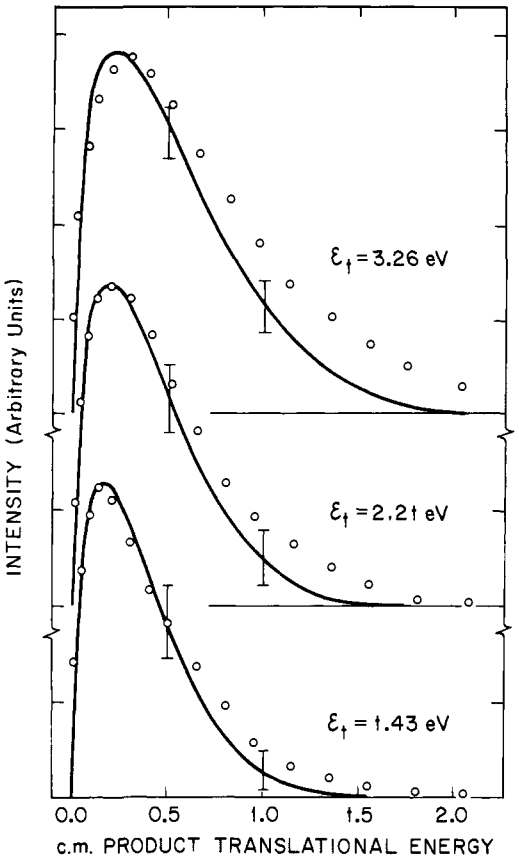

Figure 8. Plot of $\mathcal{P}(\mathcal{E}_t)$ vs. $\mathcal{E}_t$ for various $C_2H_4^{\cdot+}$ reactant ion kinetic energies. The experimental data (O) are from ref 6. The solid lines are the phase space calculations discussed in the text.

First, there could be errors in the phase space calculations above 1 eV or so due to the failure of Langevin theory to accurately predict the cross section in this energy range. These errors are not believed to be serious for the low-energy products regime where Langevin theory is still appropriate but could affect the high-energy region.

Second, the experiments may discriminate in favor of the high-energy products. We have no way of evaluating the magnitude of this effect but collection efficiencies should certainly improve for high-energy ions.

Third, the rotational energy of the products may not be distributed statistically at highest collision energies. If the orbital angular momentum of the reactants is (in part) passing preferentially to product orbital angular momentum rather than being statistically distributed between product molecular rotational states and orbital states, then the product translational energy distribution would be shifted to higher energies than predicted by statistical theory. Such an interpretation is not inconsistent with the energy dependence of the spatial product distribution. At low energies ($E \leq 1.4$ eV) the products are spherically disposed about the center of mass suggesting the complex is long lived and the products isotropically scattered in the center of mass system. At intermediate energies (1.4 eV $< E <$ 3.2 eV) the products are scattered with forward/backward symmetry about the collision axis suggesting the products are departing in the collision plane.[32] By $E = 4.1$ eV, the products are primarily forward scattered suggesting a direct mechanism dominates. Hence, it is possible that as the collision energy increases at least a fraction of the collisions occur in which the incoming orbital angular momentum passes preferentially to the product orbital angular momentum. The spatial product distribution does not require that this be the case, however.

Finally, it is possible that the vibrational energy is not randomized in the collision complex and in its subsequent decomposition to products. This was the conclusion of Lee et al.[6] A number of reasons suggest to us this is probably not the case, however. First, characteristic vibrational periods are two to three orders of magnitude shorter than rotational periods. Hence, in one rotational period hundreds, or even thousands, of vibrations can occur. It is likely, for the $C_4H_8^{\cdot+}$ intermediate considered here, that this time span is sufficient for complete anharmonic coupling of the normal modes. Second, the basis on which Lee et al. came to their conclusion is suspect. The considerable disagreement between theory and experiment cited by Lee et al.[6] clearly does not exist in the results presented here (Figure 8). The origin of the disagreement between experiment and theory suggested by Lee et al.[6] has been traced by Klots.[15b] In using the theory of Safron et al.,[16] Lee et al.[6] assumed for convenience that the total rate of decomposition of the excited complex integrated over the available energy only weakly depends on the total angular momentum of the complex. Such is simply not the case, and this assumption led to erroneous theoretical predictions by Lee et al. There is no need to assume only an "effective" number of oscillators, less than the true number, are active in the collision complex, and it is our opinion that there is no evidence that demonstrates that vibrational energy is not randomized in the ethylene system.

IV. Summary

Statistical phase space calculations have been made on the reaction of $C_2H_4^{\cdot+}$ with C_2H_4 using a theory that rigorously conserves energy and angular momentum. Comparisons have been made with experiment on the dependence of the reaction cross section on internal energy in $C_2H_4^{\cdot+}$ and on the dependence of the product translational energy distribution on $C_2H_4^{\cdot+}$ kinetic energy. The cross sectional dependence is only qualitatively consistent with phase space predictions. The experimental cross section decreases much faster with energy than predicted by theory. In our opinion the reason for the discrepancy is the cross section of the reaction is determined by the potential surface characteristics in the region of the intermediate $C_4H_8^{\cdot+}$ complex. These characteristics are completely ignored in the phase space approach which assumes reaction can be characterized solely by the properties of the separated reactants and products. An argument is made that the dependence of the cross section on energy can be accounted for by considering a competition between an isomerization reaction in the $C_4H_8^{\cdot+}$ complex and the back dissociation reaction of the complex to form the reactants. Quantitative predictions await further theoretical development. We conclude the reaction most likely proceeds according to statistical theory predictions but this suggestion remains to be demonstrated unambiguously.

The product kinetic energy distribution is well fit by the statistical phase space theory over a broad range of reactant ion kinetic energies. There are minor deviations at highest energies and several possibilities are suggested to explain these. The agreement between theory and experiment contrasts with conclusions of Lee et al.[6] who suggested vibrational energy is not randomized in the collision complex. Klots[15b] has obtained results in agreement with ours using an approximate phase space theory.

The product kinetic energy distribution primarily depends on the potential surface characteristics in the products region. Hence, it is not too surprising these results are accurately fit by the phase space theory while the cross section is not. Similar findings have been made in a number of unimolecular systems we have recently reported;[30] the energy dependence of the rate constant is not well reproduced by the phase space approach but the product kinetic energy distribution is. The rate constant

dependence on energy in these systems was well fit using RRKM theory, however, which prompted our proposed explanation of the energy dependence of the cross section in the ethylene reaction.

The diagnostic value of the statistical phase space theory should be emphasized. Because energy and angular momentum are rigorously conserved, the theory presented here serves as a limit from which the mechanism of chemical reactions can be analyzed. It is our opinion that reliable mechanistic information can be best extracted from experimental data through comparisons of that data with a theory such as the one presented here. More approximate theoretical approaches are often useful and sometimes necessary, but care must be taken to apply them properly. It is also worth noting that experimental details should be analyzed and incorporated into the theoretical analysis as accurately as possible. It is usually the case that velocity and energy distributions can be obtained that reliably reflect the experimental conditions used to obtain the data that are to be compared with theoretical predictions. The extra effort required to incorporate them into the theory should be made.

Acknowledgment. The support of the National Science Foundation under Grant MPS74-18397 is gratefully acknowledged. We would also like to thank Dr. A. D. Williamson for pointing out an error in our analysis and for providing the data used in Figure 5. The comments of a referee were also useful.

References and Notes

(1) See, for example, (a) Z. Herman, A. Lee, and R. Wolfgang, *J. Chem. Phys.*, **51**, 452 (1969); (b) J. M. Parsons, K. Shobatake, Y. T. Lee, and S. A. Rice, *Faraday Discuss. Chem. Soc.*, **55**, 344 (1973), and references therein.
(2) See, for example, J. G. Moehlmann, J. T. Gleaves, J. W. Hudgens, and J. D. McDonald, *J. Chem. Phys.*, **60**, 4790 (1974); J. T. Gleaves and J. D. McDonald, *ibid.*, **62**, 1582 (1975); J. G. Moehlmann and J. D. McDonald, *ibid.*, **62**, 3052, 3061 (1975).
(3) (a) B. Andlauer and Ch. Ottinger, *J. Chem. Phys.*, **55**, 1471 (1971); *Z. Naturforsh., A*, **27**, 293 (1972); (b) A. S. Werner and T. Baer, *J. Chem. Phys.*, **67**, 2900 (1975); (c) T. Baer, A. S. Werner, and B. P. Tsai, *ibid.*, **62**, 2497 (1975); (d) J. H. D. Eland and H. Schulte, *ibid.*, **62**, 3835 (1975).
(4) See, for example, (a) W. A. Chupka and M. E. Russell, *J. Chem. Phys.*, **48**, 1527 (1968); (b) P. R. Le Breton, A. D. Willlamson, J. L. Beauchamp, and W. T. Huntress, *ibid.*, **62**, 1623 (1975).
(5) D. T. Terwilliger, J. H. Beynon, and R. G. Cooks, *Proc. R. Soc. London, Ser. A*, **341**, 135 (1974); J. F. Elder, J. H. Beynon, and R. G. Cooks, *Org. Mass Spectrom.*, **10**, 273 (1975); R. G. Cooks, K. C. Kim, T. Keough, and J. H. Beynon, *Int. J. Mass Spectrom. Ion Phys.*, **15**, 271 (1974).
(6) A. Lee, R. L. Leroy, Z. Herman, R. Wolfgang, and J. C. Tully, *Chem. Phys. Lett.*, **12**, 596 (1972).
(7) For a recent discussion see: P. J. Kuntz, "Interactions between Ions and Molecules", P. Ausloos, Ed., Plenum Press, New York, N.Y., 1975, p 123; also see, A. Kupperman and G. C. Schatz, *J. Chem. Phys.*, **62**, 2502 (1975).
(8) H. Pelzer and E. Wigner, *Z. Phys. Chem., Abt. B*, **15**, 445 (1932); H. Eyring, M. G. Evans, and M. Polanyi, *Trans. Faraday Soc.*, **31**, 875 (1935); *J. Chem. Phys.*, **3**, 107 (1935); S. Glasstone, K. J. Laidler, and H. Eyring, "Theory of Rate Processes", McGraw-Hill, New York, N.Y., 1941.
(9) R. A. Marcus and O. K. Rice, *J. Phys. Colloid. Chem.*, **55**, 894 (1951); R. A. Marcus, *J. Chem. Phys.*, **20**, 359 (1952).
(10) See, for example, L. D. Spicer and B. S. Rabinovitch, *Annu. Rev. Phys. Chem.*, **21**, 349 (1970).
(11) P. Pechukas and J. C. Light, *J. Chem. Phys.*, **47**, 3281 (1965); J. Lin and J. C. Light, *ibid.*, **43**, 3209 (1965); P. Pechukas, J. C. Light, and C. Rankin, *ibid.*, **44**, 794 (1965); J. C. Light, *Discuss. Faraday Soc.*, **No. 44**, 14 (1967).
(12) E. Nikitin, *Theor. Eksp. Khim.*, **1**, 135, 144, 428 (1965); *Theor. Exp. Chem. (Engl. Transl.)*, **1**, 83, 90, 275 (1965).
(13) F. A. Wolf and J. L. Haller, *J. Chem. Phys.*, **52**, 5910 (1970).
(14) P. J. Dagidgion, H. W. Cruse, A. Schultz, and R. N. Zare, *J. Chem. Phys.*, **61**, 4450 (1974).
(15) (a) C. E. Klots, *J. Phys. Chem.*, **75**, 1526 (1971); *Z. Naturforsch., A*, **27**, 553 (1972); *Adv. Mass Spectrom.*, **6**, 969 (1973); (b) C. E. Klots, *J. Chem. Phys.*, **64**, 4269 (1976).
(16) S. A. Safron, N. D. Weinstein, D. R. Hershbach, and J. C. Tully, *Chem. Phys. Lett.*, **12**, 564 (1972).
(17) R. A. Marcus, *J. Chem. Phys.*, **62**, 1372 (1975).
(18) W. J. Chesnavich and M. T. Bowers, paper presented at the 23rd Annual Meeting of the American Society of Mass Spectrometry, Houston, Texas, May 1975; W. J. Chesnavich and M. T. Bowers, *J. Chem. Phys.*, submitted; W. J. Chesnavich, Ph.D. Thesis, University of California at Santa Barbara, 1976.
(19) Z. Herman, A. Lee, and R. Wolfgang, *J. Chem. Phys.*, **51**, 452 (1969).
(20) D. Bishop and K. Laidler, *J. Chem. Phys.*, **42**, 1688 (1965).
(21) (a) P. Langevin, *Ann. Chim. Phys.*, **5**, 245 (1905); (b) G. Gioumousis and D. P. Stevenson, *J. Chem. Phys.*, **29**, 294 (1958).
(22) W. J. Chesnavich and M. T. Bowers, unpublished work.
(23) A. D. Williamson, private communication.
(24) The programs for the actual calculations were written for use on an IBM 360/75 computer. The intersections $L_{\pm}$ in Figure 3 were determined using the Newton–Raphson method. All numerical integrations were performed using Gaussian quadrature. In the calculation of the product translational energy distributions a continuous approximation to the vibrational densities of states was used [G. Z. Whitten and B. S. Rabinovitch, *J. Chem. Phys.*, **41**, 1883 (1964)]. In the cross section calculations an exact counting technique was used for the vibrational densities of states [S. E. Stein and B. S. Rabinovitch, *J. Chem. Phys.*, **58**, 2438 (1972)].
(25) D. W. Turner, C. Baker, A. D. Baker, and C. R. Brundle, "Molecular Photoelectron Spectroscopy", Wiley, New York, N.Y., 1970.
(26) A discussion of energy deposition functions pertinent to this paper can be found in F. W. McLafferty, T. Wachs, C. Lifshitz, G. Innorta, and P. Irving, *J. Am. Chem. Soc.*, **92**, 6867 (1970).
(27) For a discussion of k vs. E curves of this type see M. L. Vestal, "Fundamental Processes in Radiation Chemistry", P. Ausloos, Ed., Wiley, New York, N.Y., 1968.
(28) A detailed discussion of the fragmentation of $C_4H_8^{\cdot+}$ ions of differing structure and internal energy can be found in C. Lifshitz and T. O. Tiernan, *J. Chem. Phys.*, **55**, 3555 (1971).
(29) L. Bass, W. J. Chesnavich, and M. T. Bowers, *J. Am. Chem. Soc.*, to be submitted; M. T. Bowers, W. R. Davidson, T. Su, L. Bass, P. Nielson, and D. H. Aue, 24th Annual Conference on Mass Spectrometry and Allied Topics, San Diego, Calif., May 1976.
(30) W. J. Chesnavich and M. T. Bowers, *J. Am. Chem. Soc.*, submitted; W. J, Chesnavich and M. T. Bowers, 24th Annual Conference on Mass Spectrometry and Applied Topics, San Diego, Calif., May 1976.
(31) R. Stockbauer and M. G. Ingraham, *J. Chem. Phys.*, **62**, 4862 (1975).
(32) W. B. Miller, S. A. Safron, and D. R. Hershbach, *Discuss. Faraday Soc.*, **No. 44**, 108 (1967); R. D. Levine and R. B. Bernstein, "Molecular Reaction Dynamics", Oxford University Press, New York, N.Y., 1974. See also the discussion in ref 19.